

# Directing the Structures and Collective Electronic Properties of Organic Conductors: The Interplay of $\pi$ -Overlap Interactions and Hydrogen Bonds\*\*

Karine Heuzé,<sup>[a]</sup> Marc Fourmigué,<sup>[a]</sup> Patrick Batail,<sup>\*,[a]</sup> Enric Canadell,<sup>[b]</sup> and Pascale Auban-Senzier<sup>[c]</sup>

**Abstract:** The ethylenedithiotetrathiafulvalene (EDT-TTF) directly functionalized with a primary amido group, which is both a hydrogen bond donor and acceptor group, is prepared from the corresponding ester. The electron-donating ability of EDT-TTF-CONH<sub>2</sub> (**1**), which is comparable to that of bisethylenedithiotetrathiafulvalene (BEDT-TTF) despite the presence of the electron-withdrawing amidic group, allows the successful electrocrystallization of air-stable cation radical salts. Two completely different salts are obtained with the isosteric AsF<sub>6</sub><sup>-</sup> and ReO<sub>4</sub><sup>-</sup> ions; the former has 6:1 stoichiometry, and the latter has 2:1 stoichiometry. Compound (**1**)<sub>6</sub>(AsF<sub>6</sub>) crystallizes in the *P* $\bar{3}$  space

group, and the three crystallographically independent donor molecules are linked to each other through a combination of N–H $\cdots$ O and C–H $\cdots$ O hydrogen bonds. This strong trimeric motif organizes around the AsF<sub>6</sub><sup>-</sup> ion located on the  $\bar{3}$  axis, exemplifying the templating effect of the octahedral anion on the whole structure. The presence of a uniform spin chain, as identified in the crystal structure, is confirmed by the Bonner–Fischer behavior of the mag-

netic susceptibility. In the 2:1 ReO<sub>4</sub><sup>-</sup> salt, two crystallographically independent organic slabs are interconnected through N–H $\cdots$ O(Re) hydrogen bonds, demonstrating the overlooked hydrogen-bond acceptor capability of this anion. The salt exhibits metallic behavior with a weak localization below 200 K. Both structures reveal the occurrence of a strong C–H $\cdots$ O hydrogen bond involving the aromatic CH group of the EDT-TTF core, which is activated by the neighboring amidic moiety. Together with the NH $\cdots$ O hydrogen bond, it gives rise to a cyclic motif noted R<sub>2</sub><sup>1</sup>(7) in Etter's graph set analysis.

**Keywords:** conducting materials • crystal engineering • hydrogen bonds • magnetic properties • template synthesis

## Introduction

Current research into the chemistry of molecular assemblies and crystal engineering exemplifies our increased ability to efficiently direct the construction of novel structures. This relies on the pivotal role of balanced intermolecular interactions<sup>[1]</sup> and the manipulation of hydrogen bonding preferences<sup>[2, 3]</sup> between molecular precursors.<sup>[4]</sup> In contrast, our present ability to induce, then modify, a property in a given structure or a set of structures is still in its infancy precisely because what determines the structure is not necessarily what

ultimately determines the property of the collection of objects assembled within a given structure.<sup>[5]</sup> For instance, the conductivity of molecular conductors is to a large extent determined by the nature of the energy states near the Fermi level, which usually derive from  $\pi$ -type orbitals of the donor and/or acceptor molecules. The way in which these orbitals overlap in the solid state and either spread into energy bands or remain as very localized levels is of course imposed by the crystal packing. The crystal packing itself results from a delicate balance between several contributions, the aforementioned overlap interactions on the one hand, and (C–H)<sub>donor</sub> $\cdots$ X<sub>anion</sub> hydrogen bonds (X = O, Hal),<sup>[6, 7]</sup> electrostatic and van der Waals dispersion forces on the other hand, none of which contributes to the dispersion of the  $\pi$ -type bands involved at the Fermi level. Thus, in order to build a molecular assembly with predetermined conducting properties, we must know first what type of possible packing will lead to the appropriate overlap of the  $\pi$ -type orbital of the molecular precursors, and second, how to modify and instruct the molecular units in order to direct the packing towards that required. Recent advances in the functionalization of the species commonly used in building molecular conductors

[a] Dr. P. Batail, Dr. M. Fourmigué, Dr. K. Heuzé  
Institut des Matériaux de Nantes, UMR 6502 CNRS-Université de Nantes  
2, rue de la Houssinière, BP32229, F-44322 Nantes 03 (France)  
Fax: (+33)240-373-995  
E-mail: batail@cnrs-immn.fr

[b] Dr. E. Canadell  
Institut de Ciència de Materials de Barcelona (CSIC)  
Campus de la UAB, E-08193 Bellaterra (Spain)

[c] P. Auban-Senzier  
Laboratoire de Physique des Solides  
Bât. 510, CNRS-Université Paris-Sud, F-91405 Orsay (France)

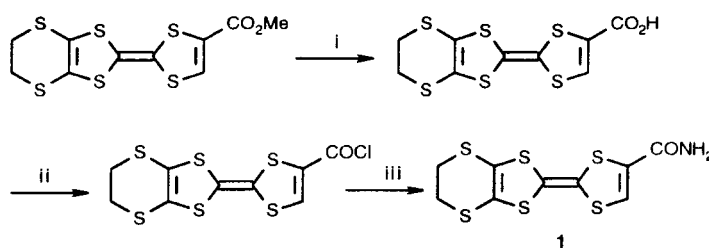
provide novel opportunities for a significant jump in the engineering of molecular conductors. Hence the need to construct novel, highly ordered electroactive molecular crystals based on new functionalized building blocks and correlate their collective electronic properties with precise structural features in order to ultimately be able to control and manipulate *both* the structure and the properties of the system.

Herein we report on two compounds in which the combination of two functionalities, HOMO–HOMO overlap interactions of conjugated cation radicals and amide hydrogen bond requirements, cooperate to accurately recognize and adjust to diverse anion symmetries. Attaching *strong* hydrogen-bond donor *and* acceptor functionalities to conjugated cores is therefore expected to critically govern the outcome of the competition between the overlap interactions of the open-shell donor molecules, which stabilize conducting stacks or slabs, and directional donor–donor as well as donor–anion hydrogen-bonding interactions at the organic–inorganic interface. Organic  $\pi$  donors derived from functionalized tetrathiafulvalene (TTF) molecules such as alcohols, [EDT-TTF-CH<sub>2</sub>OH]<sup>[8]</sup> or ( $\pm$ )Me<sub>3</sub>TTF-CHMe(OH)],<sup>[9]</sup> phosphonic acid,<sup>[10]</sup> (Me<sub>3</sub>-TTF-PO<sub>3</sub>H<sup>-</sup>) and amide<sup>[11]</sup> or thioamide (TTF-CSNHMe)<sup>[12]</sup> derivatives have been engaged in cation radical salts. We chose to functionalize the EDT-TTF core with a primary amide group (CONH<sub>2</sub>), which is both an excellent hydrogen-bond donor *and* acceptor group.<sup>[13]</sup> This was at-

tached directly on the EDT-TTF core to rigidify the molecular skeleton and hence limit the solubility<sup>[14]</sup> of the electrocrystallized salts and also to prevent unnecessary lateral extension of the functional group at the expense of optimal intermolecular  $\pi$ – $\pi$  overlap interactions. Vastly different architectures *and* electronic properties result when this redox-active primary amide, EDT-TTF-CONH<sub>2</sub> (**1**), is engaged in cation radical salts with two isosteric monoanions of different chemical nature and symmetry. This is a direct consequence of the geometric requirements imposed by the directional, selective interfacial hydrogen bonds and their associated networks.

## Results and Discussion

**Preparation of the molecules and their salts.** EDT-TTF-CONH<sub>2</sub> (**1**) is prepared from the carboxylic ester derivative<sup>[15]</sup> as shown in Scheme 1. A modification of the hydrolysis step



Scheme 1. Reagents and conditions: i) LiOH in H<sub>2</sub>O/dioxane, room temperature, 15 h; ii) oxalyl chloride, pyridine (catalytic) in THF, 45 °C, 3 h; iii) NH<sub>3</sub> in THF, 1 h.

**Abstract in French:** L'éthylènedithiotétrathiafulvalène (EDT-TTF) directement fonctionnalisé par un groupement amide primaire, qui est à la fois un donneur et un accepteur de liaison hydrogène, est préparé à partir de l'ester correspondant. Le caractère donneur d'électrons de EDT-TTF-CONH<sub>2</sub> (**1**), comparable à celui du BEDT-TTF malgré la présence du groupement amide électroattracteur, permet l'électrocrystallisation de sels d'ions radicaux stables. Deux sels totalement différents sont obtenus avec les anions isostères AsF<sub>6</sub><sup>-</sup> et ReO<sub>4</sub><sup>-</sup>, le premier de stoechiométrie 6:1, le second de stoechiométrie 2:1. (I)<sub>6</sub>(AsF<sub>6</sub>) cristallise dans le groupe d'espace P $\bar{3}$ . Trois molécules de donneur, cristallographiquement indépendantes, sont liées entre elles par un réseau de liaisons hydrogène N–H $\cdots$ O et C–H $\cdots$ O. Ce motif trimérique robuste s'organise autour de l'anion AsF<sub>6</sub><sup>-</sup> situé sur l'axe  $\bar{3}$ , illustrant le rôle de template joué par l'anion octaédrique. La présence d'une chaîne de spins uniforme, identifiée dans la structure cristalline, est confirmée par le comportement de type Bonner–Fischer de la susceptibilité magnétique. Dans le sel 2:1 avec l'anion ReO<sub>4</sub><sup>-</sup>, deux plans organiques, cristallographiquement indépendants, sont interconnectés par des liaisons hydrogène N–H $\cdots$ O(Re), mettant ainsi en évidence le caractère accepteur de l'anion ReO<sub>4</sub><sup>-</sup>. Le sel a un comportement métallique au dessus de 200 K, avec une faible localisation en dessous de cette température. Les deux structures révèlent le rôle crucial joué par une liaison hydrogène C–H $\cdots$ O forte, qui engage l'atome d'hydrogène aromatique du EDT-TTF activé par le groupement amidique en ortho. Avec la liaison hydrogène N–H $\cdots$ O, elle conduit à la formation d'un motif secondaire cyclique, noté R<sub>2</sub><sup>1</sup>(7) dans la nomenclature de Etter.

previously described by Kilburn et al.<sup>[16]</sup> afforded red needles of the corresponding carboxylic acid in 90% yield. Reaction with oxalyl chloride and pyridine as a catalyst gives the acyl chloride derivative EDT-TTF-COCl. The primary amide **1** was obtained in 92% yield by reacting a solution of EDT-TTF-COCl in THF with ammonia. Two reversible oxidation waves are observed for **1** by cyclic voltammetry at 0.53 and 0.85 V vs. SCE. The first one-electron oxidation potential of **1** is intermediate between those for EDT-TTF and BEDT-TTF under the same conditions,<sup>[17]</sup> demonstrating the limited electron-withdrawing influence of a single amidic group and the ability of **1** to be readily oxidized into air-stable cation radical salts.

**Templating effect of the octahedral AsF<sub>6</sub><sup>-</sup> ion:** Electrocrystallization of solutions of **1** in 1,1,2-trichloroethane in the presence of *n*Bu<sub>4</sub>NAsF<sub>6</sub> afforded needlelike single crystals that were formulated (EDT-TTF-CONH<sub>2</sub>)<sub>6</sub>AsF<sub>6</sub> by the resolution of their X-ray crystal structure; that is, with a 6:1 stoichiometry, which is unprecedented in this chemistry. This salt crystallizes in the trigonal system, space group P $\bar{3}$ , with three donor molecules (noted **A**, **B**, **C** in the following) at general positions in the unit cell, one AsF<sub>6</sub><sup>-</sup> ion at the origin (0,0,0) on the  $\bar{3}$  axis and one AsF<sub>6</sub><sup>-</sup> ion on the threefold axis at (1/3,2/3,z), as shown in Figure 1. The AsF<sub>6</sub><sup>-</sup> ion at (0,0,0) is surrounded by six **B** donor molecules whose ethylenic end groups encapsulate the anion within a network of C–H $\cdots$ F interactions, while the amidic moieties of nine (three each of

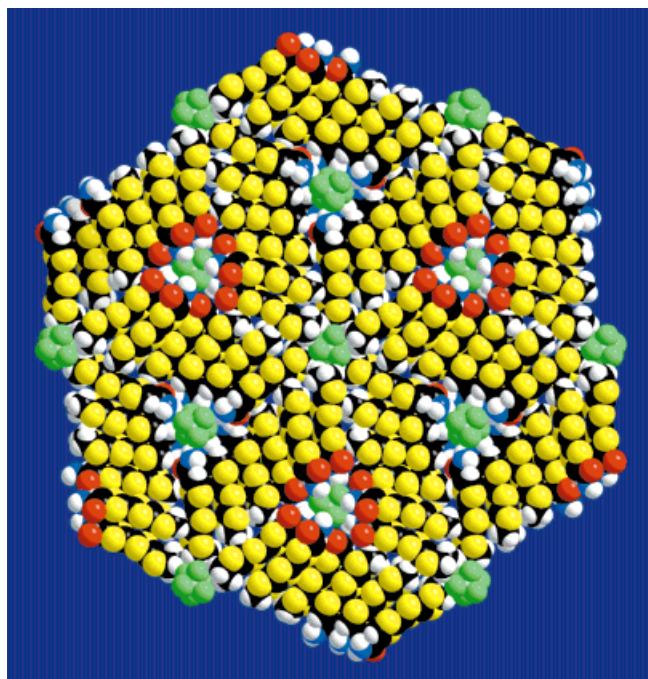


Figure 1. A projection of the structure of  $[1]_6\text{AsF}_6$  along  $[001]$ . Yellow: sulfur; red: oxygen; green: fluorine; white: hydrogen, blue: nitrogen.

**A**, **B**, and **C**) EDT-TTF- $\text{CONH}_2$  molecules are clustered around the other  $\text{AsF}_6^-$  ion located on the threefold axis. Note the spectacular segregation of the hydrophobic (EDT-TTF) and hydrophilic ( $\text{CONH}_2$ ) functionalities of **1**, which are both wrapped around  $\text{AsF}_6^-$  ions. This illustrates the ambivalent character of fluorides, which adjust to hydrophilic and hydrophobic environments.<sup>[18]</sup>

The geometrical characteristics of these interactions are given in Table 1. Two  $\text{N-H}\cdots\text{O}$  and  $\text{C-H}\cdots\text{O}$  hydrogen bonds are identified between molecules **A** and **B**, and between molecules **B** and **C**, both of which involve the oxygen atom of the amidic group as the hydrogen-bond acceptor (Figure 2). The occurrence of such  $\text{C-H}\cdots\text{O}$  bonds<sup>[19, 20]</sup> demonstrates a significant activation of the hydrogen atom, whose origin is to be found in both its position *ortho* to the amidic group and the

Table 1. Hydrogen bond characteristics in  $(1)_6\text{AsF}_6$ . Indices A, B and C refer to the three independent molecules **A**, **B**, and **C**, respectively, indices a and s refer to the antiplanar and synplanar configuration of the two hydrogen atoms of the primary amide.

	$\text{D}\cdots\text{A}$ [ $\text{\AA}$ ]	$\text{H}\cdots\text{A}$ [ $\text{\AA}$ ]	$\alpha$ [ $^\circ$ ]	$\phi$ [ $^\circ$ ]
$\text{N}_\text{A}-\text{H}_\text{Aa}\cdots\text{O}_\text{B}$	2.78(1)	2.06(1)	155.2(2)	142.2(6)
$\text{N}_\text{B}-\text{H}_\text{Ba}\cdots\text{O}_\text{C}$	2.935(9)	2.080(9)	172.3(2)	153.1(6)
$\text{C}_\text{A}-\text{H}_\text{A}\cdots\text{O}_\text{B}$	3.47(1)	2.61(1)	155.5(2)	120.8(6)
$\text{C}_\text{B}-\text{H}_\text{B}\cdots\text{O}_\text{C}$	3.182(9)	2.370(9)	145.7(2)	131.5(5)
$\text{C}_\text{C}-\text{H}_\text{C}\cdots\text{O}_\text{A}$	3.38(1)	2.63(1)	139.2(2)	152.0(6)
$\text{N}_\text{B}-\text{H}_\text{Bs}\cdots\text{F}$	3.16(1)	2.71(1)	113.8(1)	
$\text{N}_\text{B}-\text{H}_\text{Bs}\cdots\text{F}$	3.25(1)	2.41(1)	166.0(2)	
$\text{N}_\text{C}-\text{H}_\text{Cs}\cdots\text{F}$	3.08(1)	2.29(1)	152.4(2)	
$\text{N}_\text{C}-\text{H}_\text{Cs}\cdots\text{F}$	2.97(1)	2.35(1)	130.0(3)	
$\text{N}_\text{A}-\text{H}_\text{As}$ not bound				

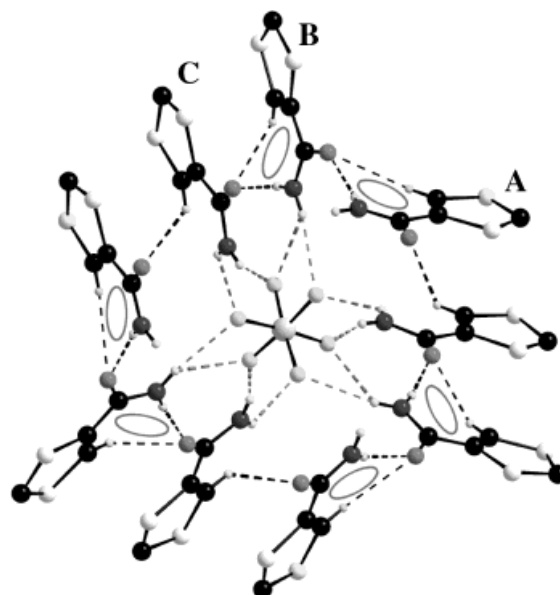
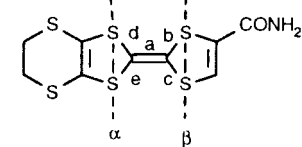


Figure 2. Projection of the hydrogen bond network around the hydrophilic threefold symmetry  $\text{AsF}_6^-$  site within  $[1]_6\text{AsF}_6$ . The gray ellipsoids symbolize the  $\text{R}_2^1(7)$  ring motifs, exemplifying the tweezer chelates connecting molecules **A** and **B** and molecules **B** and **C** within the trimeric **ABC** units. Only the dithiole rings bearing the amido groups are depicted.

cationic state of the EDT-TTF core. This *ortho* effect has already been observed in the structures of  $\alpha,\beta$ -unsaturated acids<sup>[21]</sup> and quinones,<sup>[22]</sup> while the C–H activation upon oxidation of the TTF core was revealed some years ago in the analysis of the structural transition accompanying the neutral-to-ionic transition in  $\text{TTF}\cdot\text{Chloranil}$ .<sup>[19]</sup> The *chelating* ability of this amide bearing an *ortho*-hydrogen atom gives rise to a cyclic motif, denoted  $\text{R}_2^1(7)$  in Etter's notation.<sup>[23]</sup> Thus, the robust **ABC** trimer built of two such  $\text{R}_2^1(7)$  motifs further interacts with  $\text{AsF}_6^-$  through  $\text{N-H}\cdots\text{F}$  hydrogen bonds (Table 1). By virtue of the  $\bar{3}$  site symmetry of  $\text{AsF}_6^-$ , those hydrogen-bond interactions generate a crownlike motif, which exemplifies the templating effect of the octahedral anion in directing the whole structural arrangement: the threefold symmetry of the anion is expressed throughout the whole structure through its hydrogen bonds with the amides. Note also that these precise hydrogen-bond patterns and the EDT-TTF overlap requirements cooperate and form singly oxidized, centrosymmetrical hexameric units,  $(\text{BCA}\cdots\text{ACB})^{+\cdot}$  (see Figure 1). The extent of delocalization of the positive charge on the three independent molecules within these hexamers can be ascertained by a careful analysis of the geometrical characteristics of the individual molecules, and particularly the bond lengths within the TTF core and its deviation from planarity.<sup>[24]</sup> Hence, as shown in Table 2, molecules **B** and **C** appear to be in their neutral state, while molecule **A** is partially oxidized. The title compound can thus be formulated  $(\text{A}_2)^{+\cdot}(\text{B}^0)_2(\text{C}^0)_2(\text{AsF}_6^-)$ . The analysis of the electronic structure substantiates this assignment. Within the dimeric  $(\text{A}_2)^{+\cdot}$  moiety, the two inversion-related molecules overlap in a nearly eclipsed manner (Figure 3) with a small longitudinal displacement of 0.8  $\text{\AA}$ , while the shortest intermolecular S–S distance is 3.449(8)  $\text{\AA}$ . These dimers stack along the *c* direction with a similar intermolecular S–S

Table 2. Bond lengths [Å] and torsion angles [°] within the TTF core in **1** and the three independent molecules **A**, **B**, and **C** in  $(\mathbf{1})_6\text{AsF}_6$ .



Parameters	Neutral <b>1</b>	<b>A</b>	<b>B</b>	<b>C</b>
a (C=C)	1.32(3)	1.371(9)	1.338(9)	1.335(9)
b (C-S)	1.77(2)	1.723(8)	1.765(8)	1.763(7)
c (C-S)	1.76(2)	1.748(8)	1.761(8)	1.769(7)
d (C-S)	1.75(2)	1.752(8)	1.751(8)	1.746(8)
e (C-S)	1.75(2)	1.733(8)	1.763(7)	1.758(8)
$\alpha$	15(2)	6.9(6)	18.3(5)	12.5(5)
$\beta$	4(2)	0.8(6)	1(1)	6.5(6)

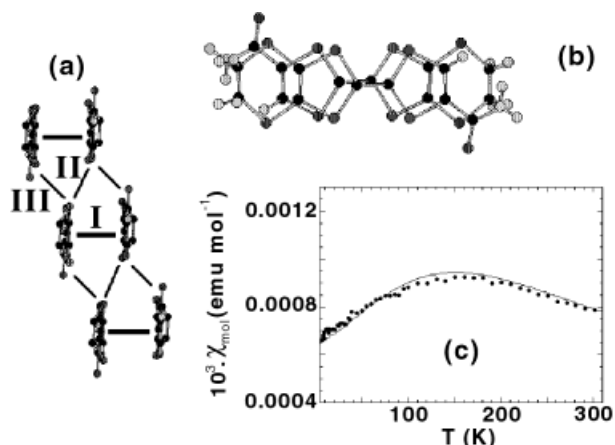


Figure 3. a) A uniform chain of  $(\mathbf{A}_2)^{2+}$  dimers in  $[\mathbf{1}]_6\text{AsF}_6$  and the corresponding HOMO–HOMO interaction energies **I**–**III** ( $\beta$ ) calculated by the extended Hückel method: **I**, 0.48, **II**, 0.017, **III**, 0.097 eV. b) Intermolecular overlap in the dimer showing a quasi-eclipsed interaction. c) Magnetic susceptibility of  $[\mathbf{1}]_6\text{AsF}_6$ . Data have been corrected for diamagnetism and a low-temperature Curie tail attributable to magnetic defaults. The solid line is a fit to the uniform spin chain model.

distance (3.442(8) Å), giving rise to uniform chains of  $(\mathbf{A}_2)^{2+}$  units, magnetically isolated from each other in the structure by the neutral **B** and **C** molecules. From an electronic point of view, this salt can thus be described as a one-dimensional chain of mixed-valence  $S = 1/2$   $(\mathbf{A}_2)^{2+}$  dimers. This is confirmed by the observed temperature dependence of its magnetic susceptibility (Figure 3c), which exhibits the characteristic Bonner–Fisher behavior of a uniform spin chain with  $J = -233$  K (0.02 eV). This salt exhibits semiconducting behavior with a sizeable room-temperature conductivity ( $\sigma_{\text{RT}} = 2 \times 10^{-2} \text{ Scm}^{-1}$ ) and an activation energy of 0.11 eV, demonstrating that this novel motif of chains of side-by-side dimers allows a sizeable electronic delocalization along the *c* axis.

**The  $\text{ReO}_4^-$  ion as hydrogen-bond acceptor.** Electrocrystallization of **1** in the presence of  $n\text{Bu}_4\text{NReO}_4$  afforded platelike crystals of the 2:1 salt  $(\mathbf{1})_2\text{ReO}_4$ . Its structure (Figure 4) appears to be vastly different from the  $\text{AsF}_6^-$  salt, primarily because the single perrhenate site accepts both amidic and ethylene end group environments. Two crystallographically independent molecules, **A** and **B**, give rise to two donor slabs,

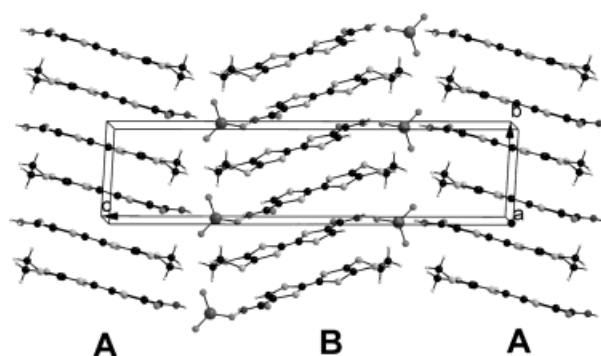
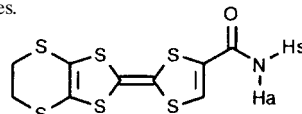


Figure 4. Alternating slabs of molecules **A** and **B** in  $[\mathbf{1}]_2\text{ReO}_4$ . Note the mixed amidic and ethylenic environments of the  $\text{ReO}_4^-$  ions.

**A** and **B**, which alternate in the *c* direction. In stark contrast with the structure encountered for  $(\mathbf{1})_6\text{AsF}_6$ , the chelating amide no longer points toward the oxygen atom of another amidic group, but, instead, reaches solely for the oxygen atoms of the  $\text{ReO}_4^-$  ion (Table 3). The latter anion would thus

Table 3. Hydrogen bond characteristics in  $(\mathbf{1})_2\text{ReO}_4$ . Indices **A** and **B** refer to the two independent molecules **A** and **B**, respectively, indices *a* and *s* refer to the antiplanar and synplanar configuration of the two hydrogen atoms of the amides.



	D...A [Å]	H...A [Å]	$\alpha$ angle
$\text{N}_\text{A}-\text{H}_\text{As} \cdots \text{O}(\text{Re})$	2.95(1)	2.09(1)	171.4(4)
$\text{N}_\text{A}-\text{H}_\text{As} \cdots \text{O}(\text{Re})$	3.06(1)	2.36(1)	138.3(4)
$\text{N}_\text{B}-\text{H}_\text{Bs} \cdots \text{O}(\text{Re})$	3.02(1)	2.23(1)	152.9(3)
$\text{N}_\text{B}-\text{H}_\text{Ba} \cdots \text{O}(\text{Re})$	2.91(1)	2.07(1)	166.4(3)
$\text{C}_\text{A}-\text{H}_\text{A} \cdots \text{O}(\text{Re})$	3.64(1)	2.76(1)	158.4(3)
$\text{C}_\text{B}-\text{H}_\text{B} \cdots \text{O}(\text{Re})$	3.41(1)	2.52(1)	158.4(3)

appear to be a stronger hydrogen-bond acceptor than the organic carbonyl group. As shown in Figure 5, the  $\text{R}_2^1(7)$  chelate rings are again observed but in this case link two donor molecules to two oxygen atoms of a single  $\text{ReO}_4^-$  ion. The remaining two (N–)H atoms of the **A** and **B** amides are engaged with another  $\text{ReO}_4^-$  ion, giving rise to a larger ring motif, which involves two donor molecules and two anions, noted  $\text{R}_4^3(10)$  in Figure 5. This salient templating effect of the isosteric  $\text{AsF}_6^-$  and  $\text{ReO}_4^-$  ions unambiguously demonstrates the determining role played by the hydrogen-bonding functionality of **1** in the structural organization of its salts. The

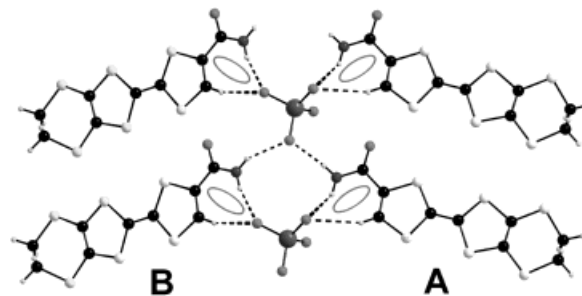


Figure 5. Hydrogen bond network in the  $[\mathbf{1}]_2\text{ReO}_4$  salt. The  $\text{R}_2^1(7)$  graph set appears with gray ellipsoids.

recurrent observation of the  $R_2^1(7)$  motif confirms the importance of C–H $\cdots$ O bonds in these structures. Furthermore, the differences between the two structures highlight the strong hydrogen-bond acceptor character of the  $\text{ReO}_4^-$  ion which favorably competes with carbonyl oxygen atoms, a significant structure-directing capability of this anion.

As already mentioned, two crystallographically independent donor planes **A** and **B**, of the  $\beta$  type,<sup>[25]</sup> have been identified. The similarity of the central C=C bond lengths and results of the analysis of the electronic structure<sup>[26]</sup> of the two donor planes clearly show that the charge of both donor molecules **A** and **B** must be identical; that is,  $+1/2$ . The calculated intermolecular HOMO–HOMO interaction energies<sup>[27]</sup> differ however significantly within each plane. Within plane **A**, sizeable interactions are observed between one given molecule and each of its nearest neighbors (Figure 6a). In

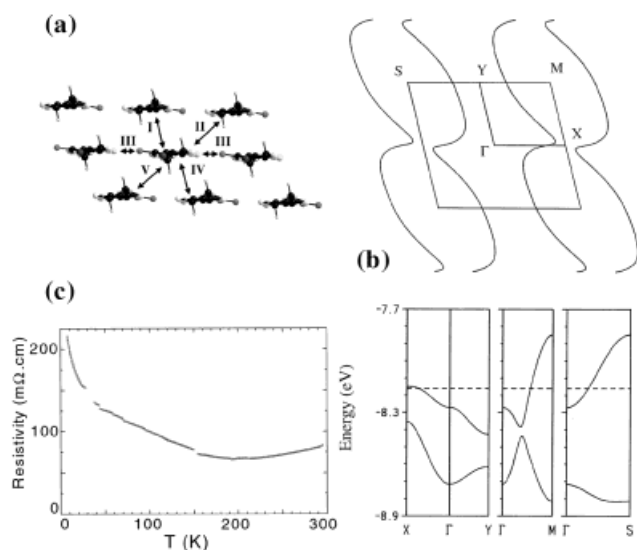


Figure 6. a) Side view of the plane of molecules **A** and the HOMO–HOMO interaction energies ( $\beta$ ) calculated by the extended Hückel method: **I**, 0.02; **II**, 0.25; **III**, 0.14; **IV**, 0.20; **V**, 0.26 eV. b) Calculated band structure and Fermi surface associated with the donor plane **A** in  $[\mathbf{1}]_2\text{ReO}_4$  assuming a  $+1/2$  charge for the donor molecule.  $\Gamma$ , X, Y, M and S refer to the (0,0),  $(a^*/2,0)$ ,  $(0,b^*/2)$ ,  $(a^*/2,b^*/2)$  and  $(-a^*/2,-b^*/2)$  wave vectors, respectively. c) Temperature dependence of the conductivity of  $[\mathbf{1}]_2\text{ReO}_4$  at ambient pressure.

plane **B**, the donor molecules are strongly associated into discrete dimeric units. As a consequence, two bands of strong dispersion, the upper one of which is half-filled, are found in plane **A**. The calculated Fermi surface (Figure 6b) can be described as arising from the superposition of a series of ellipses. Although strictly speaking the Fermi surface is open, it is clearly associated with two-dimensional metallic behavior. In contrast, the band structure of plane **B** is made up from two well-separated bands (reflecting the strong dimerization) with a small dispersion (0.2 eV). This strongly suggests that the electrons in this plane are localized within essentially noninteracting dimers. Single-crystal conductivity measurements confirm (Figure 6c) the metallic behavior ( $\sigma_{RT} = 14 \text{ S cm}^{-1}$ ) and show a localization around 200 K where the salt becomes semiconducting with a very small activation energy (0.3 meV). As a consequence, the conductivity of this

rare structure of alternating conducting and insulating planes is nearly constant in the whole temperature range. It is therefore tempting to predict that small changes such as substituting  $\text{ReO}_4^-$  by  $\text{ClO}_4^-$  or alloying, or the application of an external pressure might have a strong effect on the transport properties of this salt.

## Conclusion

By creating situations where strong, directional hydrogen-bond interactions are allowed to compete with intermolecular overlap interactions between open-shell cation radicals, one observes a remarkable, balanced synergy where both structural principles cooperate in the construction of unprecedented hydrogen-bonded architectures blessed with collective solid-state electronic properties. This cooperative behavior is rooted in the fact that the actual energy scales of these interactions are such that none of them is able to clearly dominate the final structure. The principle of *selectivity in counter-anion recognition* illustrated by the results reported herein is both remarkable and unprecedented in the chemistry of electroactive molecular materials.<sup>[28]</sup> Also, the occurrence of strong C–H<sub>ortho</sub> $\cdots$ O hydrogen bonds, enhanced by the cationic state of the TTF core, revealed the robust chelating cyclic  $R_2^1(7)$  motif, a novel construction tool in the chemistry of molecular assemblies. In this respect, the potential of the  $\text{ReO}_4^-$  ion as a strong hydrogen-bond acceptor is expected to find interesting applications in the development of anion receptors<sup>[29]</sup> as well as the template synthesis of molecular networks.

## Experimental Section

**EDT-TTF-COCl:** Oxalyl chloride (0.4 mL, 4.62 mmol) and pyridine (1  $\mu\text{L}$ ) were added to a stirred solution of the acid EDT-TTF-CO<sub>2</sub>H (**6**)<sup>[16]</sup> (0.55 g, 1.5 mmol) in THF (60 mL) under nitrogen at 45 °C. The mixture was stirred for 3 h and filtered, the volume was reduced to 10 mL and the product was precipitated by addition of dry hexane to afford the acid chloride **7** as a purple microcrystalline powder (0.55 g, 94 %). M.p. 165–168 °C (decomp); elemental analysis (%) calcd for  $\text{C}_9\text{H}_5\text{OS}_6\text{Cl}$ : C 30.28, H 1.41, S 53.89, Cl 9.93; found C 30.65, H 1.41, S 51.73, Cl 10.17; IR (KBr):  $\tilde{\nu} = 1710$  (CO)  $\text{cm}^{-1}$ ; <sup>1</sup>H NMR (200 MHz,  $\text{CDCl}_3$ ):  $\delta = 7.78$  (s, 1H; C=CH), 3.31 (s, 4H;  $\text{CH}_2-\text{CH}_2$ ); MS:  $m/z$  (%): 356 [ $M^+$ ] (85), 328 [ $M^+ - \text{CH}_2 - \text{CH}_2$ ] (72).

**EDT-TTF-CO<sub>2</sub>NH<sub>2</sub>:** A solution of the acid chloride **7** (150 mg, 0.42 mmol) in dry THF (10 mL) was added dropwise to a  $\text{NH}_3$  saturated THF solution (10 mL). The solution turned yellow and was stirred for 1 h, filtered, and concentrated to afford **1** as red needles after recrystallization from THF (130 mg, 92 %). M.p. 214–215 °C (decomp); elemental analysis (%) calcd for  $\text{C}_9\text{H}_7\text{ONS}_6 \cdot \text{THF}_{0.75}$ : C 33.78, H 2.55, N 3.94, S 56.83; found C 33.17, H 2.72, N 3.71, S 52.56; IR (KBr):  $\tilde{\nu} = 3417-3173$  ( $\text{NH}_2$ ), 1647 (C=O)  $\text{cm}^{-1}$ ; UV/Vis (THF):  $\lambda_{\text{max}}$  ( $\epsilon$ ) = 395 nm ( $1.9 \times 10^3 \text{ dm}^3 \text{ mol}^{-1} \text{ cm}^{-1}$ ); <sup>1</sup>H NMR (200 MHz,  $[\text{D}_6]\text{DMSO}$ ):  $\delta = 7.95$  (s, 1H;  $\text{NH}_2$ ), 7.55 (s, 1H; C=CH), 3.38 (s, 4H;  $\text{CH}_2-\text{CH}_2$ ); <sup>13</sup>C NMR (50 MHz,  $[\text{D}_6]\text{DMSO}$ ):  $\delta = 160.35$  (C=O), 134.25 (C–O), 125.04 (=CH), 103.38–113.02 (C=C), 29.47 ( $\text{CH}_2-\text{CH}_2$ ); MS:  $m/z$  (%): 337 [ $M^+$ ] (100), 309 [ $M^+ - \text{CH}_2 - \text{CH}_2$ ] (84).

**Cyclic voltammetry:** Experiments were performed at 25 °C in acetonitrile with  $n\text{Bu}_4\text{NPF}_6$  ( $5 \times 10^{-2} \text{ mol L}^{-1}$ ) as electrolyte.

**X-ray diffraction studies:** Data were collected on an imaging plate diffraction system (IPDS-Stoe). The structures were solved by direct methods and refined against  $F^2$  using the SHELXTL5.04 set of programs.<sup>[30]</sup> All non-hydrogen atoms were refined anisotropically; the H atoms were introduced at calculated positions and not refined. X-ray data for  $(\mathbf{1})_6\text{AsF}_6$ :

$C_{34}H_{42}AsF_6N_6O_6S_{36}$ ,  $M_r = 2214.252$ , crystal dimensions  $0.24 \times 0.04 \times 0.04$  mm, trigonal, space group  $P\bar{3}$ ,  $a = 33.120(5)$ ,  $c = 6.440(1)$  Å,  $Z = 3$ ,  $\rho_{\text{calc}} = 1.803$  Mg cm $^{-3}$ ,  $\lambda = 0.71073$  Å,  $T = 293(2)$  K,  $\mu(\text{Mo}_{\text{K}\alpha}) = 1.404$  mm $^{-1}$ , 214 exposures,  $\varphi$  increment  $0.7^\circ$ , 10 mm per exposure, 35747 collected reflections ( $1.88^\circ \leq \theta \leq 25.88^\circ$ ), of which 7851 independent reflections ( $R_{\text{int}} = 0.231$ ), and 2560 reflections with  $I > 2\sigma(I)$  for 493 parameters. No absorption correction was applied.  $RI = \sum ||F_o| - |F_c|| / \sum |F_o| = 0.056$  and  $wR2 = [\sum w(F_o^2 - F_c^2)^2 / \sum w(F_c^2)^2]^{1/2} = 0.060$  (all data), GOF = 0.726, largest peak and hole in final difference map, 0.68 and  $-0.60$  e Å $^{-3}$ . X-ray data for  $(\text{I})_2\text{ReO}_4$ :  $C_{18}H_{14}N_2O_6\text{ReS}_{12}$ ,  $M_r = 925.23$ , crystal dimensions  $0.34 \times 0.04 \times 0.04$  mm, triclinic, space group  $P\bar{1}$ ,  $a = 6.6031(13)$ ,  $b = 7.350(2)$ ,  $c = 29.901(6)$  Å,  $\alpha = 89.89(3)$ ,  $\beta = 85.26(3)$ ,  $\gamma = 75.93(3)^\circ$ ,  $Z = 2$ ,  $\rho_{\text{calc}} = 2.191$  Mg cm $^{-3}$ ,  $\lambda = 0.71073$  Å,  $T = 293(2)$  K,  $\mu(\text{Mo}_{\text{K}\alpha}) = 5.267$  mm $^{-1}$ ; 313 exposures,  $\varphi$  increment  $0.8^\circ$ , 3 mm per exposure, 12860 collected reflections ( $2.05 \leq \theta \leq 25.80^\circ$ ), of which 5019 independent reflections ( $R_{\text{int}} = 0.156$ ), and 2374 reflections with  $I > 2\sigma(I)$  for 340 parameters. Numerical absorption correction using crystal faces (FACEIT-Stoe) was applied,  $T_{\text{min}} = 0.551$ ,  $T_{\text{max}} = 0.958$ .  $RI = \sum ||F_o| - |F_c|| / \sum |F_o| = 0.0693$  and  $wR2 = [\sum w(F_o^2 - F_c^2)^2 / \sum w(F_c^2)^2]^{1/2} = 0.0979$  (all data), GOF = 0.649, largest peak and hole in final difference map, 0.42 and  $-0.37$  e Å $^{-3}$ . Crystallographic data (excluding structure factors) for the structures reported in this paper have been deposited with the Cambridge Crystallographic Data Centre as supplementary publication no. CCDC-114717 and CCDC-114718. Copies of the data can be obtained free of charge on application to CCDC, 12 Union Road, Cambridge CB2 1EZ, UK (fax: (+44)1223-336-033; e-mail: deposit@ccdc.cam.ac.uk).

## Acknowledgments

We gratefully acknowledge financial support from the French Ministry of Education (K.H.), the CNRS and the Région Pays de la Loire. Part of this work was supported by DGES-Spain (PB96-0859) and Generalitat de Catalunya (1997 SGR 24).

- [1] a) G. Desiraju, *Chem. Commun.* **1997**, 1475–1482; b) G. Desiraju, *Angew. Chem.* **1989**, *107*, 2541–2558; *Angew. Chem. Int. Ed.* **1995**, *34*, 2311–2327.
- [2] J. Bernstein, M. C. Etter, L. Leiserowitz, in *Structure Correlation* (Eds.: H.-B. Bürgi, J. D. Dunitz), VCH, Weinheim, **1994**, ch. 11.
- [3] T. Martin, U. Obst, J. Rebek, Jr., *Science* **1998**, *281*, 1842–1845.
- [4] a) D. S. Lawrence, T. Liang, M. Levett, *Chem. Rev.* **1995**, *95*, 2229–2260; b) D. Philp, J. F. Stoddart, *Angew. Chem.* **1996**, *108*, 1242–1286; *Angew. Chem. Int. Ed. Engl.* **1996**, *35*, 1155–1196; c) J.-M. Lehn, *Supramolecular Chemistry: Concepts and Perspectives*, VCH, Weinheim, **1995**; d) O. Felix, M. W. Hosseini, A. De Cian, J. Fischer, *Angew. Chem.* **1997**, *109*, 83–85; *Angew. Chem. Int. Ed.* **1997**, *36*, 102–104.
- [5] J. D. Martin, E. Canadell, J. Y. Becker, J. Bernstein, *Chem. Mater.* **1993**, *5*, 1199–1203.
- [6] M.-H. Whangbo, D. Jung, J. Ren, M. Evain, J. J. Novoa, F. Mota, S. Alvarez, J. M. Williams, M. A. Beno, A. M. Kini, H. H. Wang, J. R. Ferraro, in *The Physics and Chemistry of Organic Superconductors* (Eds.: G. Saito, S. Kagoshima), Springer, Berlin, **1990**, pp. 262–266.
- [7] M.-H. Whangbo, J. M. Williams, A. J. Schultz, T. J. Emge, M. A. Beno, *J. Am. Chem. Soc.* **1987**, *109*, 90–94.
- [8] P. Blanchard, K. Boubekeur, M. Sallé, G. Duguay, M. Jubault, A. Gorgues, J. D. Martin, E. Canadell, P. Auban-Senzier, D. Jérôme, P. Batail, *Adv. Mater.* **1992**, *4*, 579–581.
- [9] A. Dolbecq, M. Fourmigué, P. Batail, C. Coulon, *Chem. Mater.* **1994**, *6*, 1413–1418.
- [10] A. Dolbecq, M. Fourmigué, F. C. Krebs, P. Batail, E. Canadell, R. Clérac, C. Coulon, *Chem. Eur. J.* **1996**, *2*, 1275–1282.
- [11] G. Ono, A. Izuoka, K. Tanaka, M. Mizutani, *Synth. Metals* **1993**, *55–57*, 2007–2012.
- [12] a) A. S. Batsanov, M. R. Bryce, G. Cooke, J. N. Heaton, J. A. K. Howard, *J. Chem. Soc. Chem. Commun.* **1993**, 1701–1702; b) A. J. Moore, M. R. Bryce, A. S. Batsanov, J. N. Heaton, C. W. Lehman, J. A. K. Howard, N. Robertson, A. E. Underhill, I. F. Perepichka, *J. Mater. Chem.* **1998**, *8*, 1541–1550.
- [13] a) R. Taylor, O. Kennard, W. Versichel, *J. Am. Chem. Soc.* **1983**, *105*, 5761–5766; b) R. Taylor, O. Kennard, W. Versichel, *J. Am. Chem. Soc.* **1984**, *106*, 244–248.
- [14] For a review on electrocrystallization, see: P. Batail, K. Boubekeur, M. Fourmigué, J.-C. P. Gabriel, *Chem. Mater.* **1998**, *10*, 3005–3015.
- [15] P. Blanchard, M. Sallé, G. Duguay, M. Jubault, A. Gorgues, *Tetrahedron Lett.* **1992**, *33*, 2685–2688.
- [16] R. P. Parg, J. D. Kilburn, M. C. Petty, C. Pearson, T. G. Ryan, *J. Mater. Chem.* **1995**, *5*, 1609–1615.
- [17] EDT-TTF oxidizes at 0.44 and 0.75, BEDT-TTF at 0.56 and 0.80 V vs. SCE under the same conditions.
- [18]  $\text{PF}_6^-$  or  $\text{AsF}_6^-$  are found in highly hydrophilic cavities in their acid form which crystallize as clathrate hydrates encapsulating the anion: a) D. Mootz, E. J. Oellers, M. Wiebcke, *J. Am. Chem. Soc.* **1987**, *109*, 1200–1202; b) M. Wiebcke, D. Mootz, *Z. Krist.* **1988**, *183*, 1–13. Hydrophobic environments are found, for example, in the structures of the Bechgaard salts such as  $(\text{TMTSF})_2\text{AsF}_6$ : a) K. Bechgaard, C. S. Jacobsen, K. Mostensen, H. J. Pedersen, N. Thorup, *Solid State Commun.* **1980**, *33*, 1119–1125; b) M. A. Beno, G. S. Blackman, P. C. W. Leung, J. M. Williams, *Solid State Commun.* **1983**, *48*, 99–103.
- [19] P. Batail, S. J. LaPlaca, J. J. Mayerle, J. B. Torrance, *J. Am. Chem. Soc.* **1981**, *103*, 951–953.
- [20] a) G. Desiraju, *Acc. Chem. Res.* **1993**, *24*, 290–296; b) A. Gavezotti, *J. Phys. Chem.* **1991**, *95*, 8948–8955; c) R. Taylor, O. Kennard, *J. Am. Chem. Soc.* **1982**, *104*, 5063–5070.
- [21] L. Leiserowitz, *Acta Crystallogr. Sect. B* **1976**, *32*, 775–802.
- [22] J. Bernstein, M. D. Cohen, L. Leiserowitz in *The Chemistry of the Quinoid Compounds, Part I* (Ed.: S. Patai), Interscience, New York, **1974**, pp. 37–110.
- [23] a) M. C. Etter, J. C. Mc Donald, *Acta Crystallogr. Sect. B* **1990**, *46*, 256–262; b) M. C. Etter, *Acc. Chem. Res.* **1990**, *23*, 120–126; c) M. C. Etter, *J. Phys. Chem.* **1991**, *95*, 4601–4610.
- [24] Oxidized TTF moieties are well known to exhibit a lengthening of the central C=C bond with a concomitant shortening of the C–S bonds, while the two dithiole rings, often folded along the S–S axis in the neutral state, become fully planar in mixed-valence salts. See: a) A. Pénicaut, P. Batail, P. Davidson, A.-M. Levelut, C. Coulon, C. Perrin, *Chem. Mater.* **1990**, *2*, 117–123; b) P. Guionneau, C. J. Kepert, D. Chasseau, M. R. Truter, P. Day, *Synth. Metals* **1997**, *86*, 1973–1974.
- [25] The  $\alpha$ -,  $\beta$ -, and  $\kappa$ -phase denominations refer to the geometrical patterns observed for the organic slabs in BEDT-TTF salts in which molecules of one stack form a marked dihedral angle with molecules on the adjacent stack ( $\alpha$ ); the molecules on adjacent stacks are parallel ( $\beta$ ); the slab is paved with twisted donor dimers instead ( $\kappa$ ): J. M. Williams, J. R. Ferraro, R. J. Thorn, K. D. Carlson, U. Geiser, H. H. Wang, A. M. Kini, M.-H. Whangbo in *Organic Superconductors (Including Fullerenes): Synthesis, Structure, Properties and Theory*, Prentice-Hall, Inc., Englewood Cliffs, New Jersey, **1992**, p. 81.
- [26] Both the molecular and tight-binding calculations used an extended Hückel type Hamiltonian [M.-H. Whangbo, R. Hoffmann, *J. Am. Chem. Soc.* **1978**, *100*, 6093–6098] and a basis set of double- $\zeta$  Slater-type orbitals for all atoms except hydrogen. The non-diagonal  $H_{mn}$  matrix elements were calculated according to the modified Wolfsberg-Helmholz formula [J. H. Ammeter, H.-B. Bürgi, J. Thibeault, R. Hoffmann, *J. Am. Chem. Soc.* **1978**, *100*, 3686–3692].
- [27] M.-H. Whangbo, J. M. Williams, P. C. W. Leung, M. A. Beno, T. J. Emge, H. H. Wang, *Inorg. Chem.* **1985**, *24*, 3500–3502.
- [28] The Bechgaard salts, based on fully methylated  $\pi$ -donor molecules such as TMTSF or TMTTF typically adopt the same structure regardless of the nature of isosteric anions such as  $\text{BF}_4^-$ ,  $\text{ClO}_4^-$ ,  $\text{ReO}_4^-$ ,  $\text{PF}_6^-$ ,  $\text{AsF}_6^-$ ,  $\text{SbF}_6^-$ ,  $\text{NO}_3^-$ , and  $\text{Br}^-$ : a) G. Brun, B. Liautaud, S. Peytavin, M. Maurin, E. Torrelles, J. M. Fabre, L. Giral, J. L. Galigné, *J. Phys. (Paris) Colloq.* **1977**, *38*, 266–269; b) K. Bechgaard, C. S. Jacobsen, K. Mortensen, H. J. Pedersen, N. Thorup, *Solid State Commun.* **1980**, *33*, 1119–1125.
- [29] B. Dietrich, *Pure Appl. Chem.* **1993**, *65*, 1457–1464.
- [30] G. M. Sheldrick, SHELXTL version 5.04, Siemens Analytical X-Ray Instruments, Madison, Wisconsin, USA.

Received: April 30, 1999 [F 1760]